Results in Physics 17 (2020) 103062

Contents lists available at ScienceDirect

Results in Physics

journal homepage: www.elsevier.com/locate/rinp

Open-cell tungsten nanofoams: Chloride ion induced structure modification and mechanical behavior

Mingyue Zhao[a,*], Manuel J. Pfeifenberger[b], Daniel Kiener[a]

[a] Chair of Materials Physics, Montanuniversität Leoben, 8700 Leoben, Austria
[b] Erich Schmid Institute of Materials Science, Austrian Academy of Sciences, 8700 Leoben, Austria

ARTICLE INFO

Keywords:
Porous materials
Tungsten
Diffusion
Microstructure
Indentation

ABSTRACT

In this work, a nanoporous structure composed entirely of tungsten ligaments was synthesized by selective phase dissolution of a nanocrystalline tungsten-copper composite in ferric chloride aqueous solution at room temperature. Observation of the tungsten nanoligament modifications in both ferric chloride and hydrochloric acid solution illustrated that the chloride ions accelerate the surface diffusivity of tungsten atoms by two orders of magnitude, thus causing an evolution of the tungsten nanoligaments upon reconstruction and growth with the increase of dissolution time. Using nanoindentation and Vickers' microhardness measurements, we discovered that the created tungsten foam deforms via a fast densification in combination with the formation of cracks due to a low ligament strength.

Introduction

Metallic foams, i.e., porous metals, are presently the focus of very active research and development activities in numerous industrial applications such as light-weight optics, biomedical implants, high temperature filters, electrodes, electromagnetic shields, sound absorption materials, catalysts and heat exchangers [1]. Generally, in comparison to other porous materials (including plastic, glass and ceramic), porous metals have an integrative advantage in their physical and mechanical properties, including a high electrical or thermal conductivity, superior structural stability at high temperatures, good thermal shock resistance, high mechanical strength and toughness [1]. In general, there are three different types of metallic foams based on the pore structures: open cell, closed cell, and a combination of the two [2]. Closed-cell metallic foams, which do not allow access to their internal surface, are mostly used in structural, load-bearing applications, as they have good mechanical properties. In contrast, open-cell metallic foams are permeable and have very high surface areas as required for flow-through applications or when surface exchange is involved.

Tungsten (W) owns the highest melting temperature among all metals, a low coefficient of thermal expansion, a high density and superior strength [3]. Hence, W foams are dominantly applied as high current density cathodes in high power lamps [4], radiation shields against gamma and X-rays [5], or engineering and structural materials with excellent dynamic compressive properties [6]. For the function of a porous W cathode, homogeneous distribution of open pore channels is essential, as it will be impregnated with electron emissive material [7,8]. Upon emission, the emissive material, which evaporates during the formation of the current, can be constantly supplied to the surface through the open pore channels so that the cathode functions continuously. In addition, by infiltrating the empty open pores with elements of low atomic number, such as compounds of hydrogen and boron, which are preferable for stopping neutron irradiation, the open-cell porous W has potential for application in radiation shielding against neutrons [9].

Porous W is mainly processed by powder metallurgy (PM). However, in PM processing, it is difficult to control the porosity and the ratio of opening pores [10]. Chemical vapor deposition (CVD) is another common preparation method for W [11,12]. It has the advantage of forming porous W with controllable pore distribution and pore sizes across several hundreds of micrometers. Tape-casting (TC) is generally used to form thin and flat metallic sheets on a large scale [13]. By applying this method, bulk porous W with an open, biporous structure and pore sizes down to 3–6 μm was produced [13]. The aim of our work is to tailor open-cell nanoporous (np) W, as np metals possess exceptionally high mechanical strength [14,15] and radiation tolerance [16-18] compared to conventional metal foams. In addition, the nanopores can limit the evaporation rate of the emissive materials, thus possibly prolonging the lifetime of porous W cathodes [8]. As described above, it is challenging to tailor W foams with pore sizes in a nanometer

* Corresponding author at: Chair of Materials Physics, Montanuniversität Leoben, Jahnstraße 12, 8700 Leoben, Austria.
E-mail address: mingyue.zhao@unileoben.ac.at (M. Zhao).

https://doi.org/10.1016/j.rinp.2020.103062
Received 24 January 2020; Received in revised form 13 March 2020; Accepted 14 March 2020
Available online 24 March 2020

range by using PM, CVD or TC. Therefore, new fabrication techniques are required.

For the fabrication of open-cell np materials, the most common method is electrochemical dealloying (ECD), by which a less-noble component is selectively dissolved from a precursor alloy due to the standard electrode potential difference between the constituent elements [19,20]. This typically restricts the application of the method to noble metals and similarly corrosion resistant metals (e.g. Au [19-21], Ag [22] and Cu [23]). The liquid–metal dealloying (LMD) is a recently developed method, which utilizes the miscibility difference between alloy components and metallic melts to produce np metals, e.g., np Ti [24,25], Nb [26] and Si [27]. However, coarsening of the nanoporous strucutres probably can take place because of the very high dealloying temperatures. Additionally, chemical etching is required to remove the melts that are solidified in the pores. Another possibility is the vapor-phase dealloying (VPD) method. Depending on the vapor pressure difference between solid elements, nanoporous structure can be formed by evaporating one component from alloy [28]. This method is suitable for refractory metals (e.g. Nb, Ta, Mo, V, etc) that may be susceptible to oxidation during ECD and is also capable to yield small ligament sizes that are difficult to achieve via liquid metal dealloying. However, the produced porous film layers are limited to hundreds of nanometers and the sacrificial elements are not fully removed [28]. In our previous work, a unique route involving severe plastic deformation (SPD) of a coarse-grained immiscible tungsten-copper (W-Cu) composite followed by selective dissolution of the nobler Cu was developed [29]. When using ammounium persulfate ($(NH_4)_2S_2O_8$) as etchant, this technique allows for producing W nanofoams with entirely interconnected open pores, which would not be possible for ECD, LMD and CVD techniques. Furthermore, this approach can be applied to bulk composite systems and yields pure porous structures with a thickness that is challenging to achieve via VPD. Similar to ammonium persulphate ($(NH_4)_2S_2O_8$) etchant (see Ref. [29]), iron chloride ($FeCl_3$) can dissolve the nobler Cu phase while leaving the less noble W unattacked as well. In addition, $FeCl_3$ has several advantages over $(NH_4)_2S_2O_8$, such as controlled process parameters (e.g. pH value), stable effectiveness over a long term storage, low product price and low harmfulness to human health. Therefore, in this work we tailor np W by selective dissolution of the nobler Cu phase in $FeCl_3$ etching solution from a W-Cu nanocomposite. Based on characterization of the resulting porous structures by scanning electron microscopy (SEM), and mechanical tests by depth-sensing nanoindentation and Vicker's microhardness measurements, the following two open questions are addressed: (i) How does the porous structure evolve during the selective dissolution in $FeCl_3$ solution? (ii) What is the mechanical behavior of the created nanofoams under compressive stress? By taking the np W created by using $(NH_4)_2S_2O_8$ etchant [29] as a reference, the influence of the two etchants on the microstructure modifications and the corresponding evolution mechanisms of the porous structure are elucidated.

Experimental procedures

Starting material is a nanocrystalline (nc) W-Cu composite, which was acquired via high pressure torsion (HPT) of a coarse-grained W-20 wt% Cu composite ($W_{65}Cu_{35}$ in volume ratio and $W_{58}Cu_{42}$ in atomic ratio) followed by heat treatment at 300°C in a vacuum furnace for 1 h to reduce the amount of forced mechanical mixing between W and Cu. We have demonstrated that such a W:Cu ratio allows the creation of a network of entirely open pores [29]. A detailed introduction to the HPT procedure of coarse-grained W-Cu composite can be found in Ref. [30,31]. The starting material is comprised of equiaxed W grains with an average size of 15 nm and interconnected Cu phases with 20 nm on average [29]. High resolution transmission electron microscopy (HR-TEM) analysis in Ref. [29] revealed that the starting material contains three different types of interfaces, i.e., oxygen-free and low defective W grain boundaries (GBs), W GBs decorated by Cu and O atoms, and W/Cu phase boundaries (PBs) with a trace amount of O. W moving entities (including adatoms, step adatoms and kink atoms described in the terrace ledge kink model [32]) will be formed once Cu and O atoms at the latter two interfaces are removed [29].

Table 1
Parameters used for nanoporous W synthesis by selective phase dissolution in a concentrated $FeCl_3$ aqueous solution at room temperature.

Etching solution	$FeCl_3$ solution (pH < 2, 5.5 mol/L)
Etching mechanism	$FeCl_3 + Cu \rightarrow FeCl_2 + CuCl$; $FeCl_3 + CuCl \rightarrow FeCl_2 + CuCl_2$; $CuCl_2 + Cu \rightarrow 2CuCl$
Etching time	1/6 HPT disk: 1 h, 2 h, 4 h, 18 h

Nanoporous W was developed by selective phase dissolution of the starting material in a concentrated $FeCl_3$ aqueous solution (Table 1, $FeCl_3$, 5.5 mol/L) at room temperature (RT). To suppress the hydrolysis of Fe^{3+} ions, hydrochloric acid (HCl) was added into the $FeCl_3$ solution to maintain a pH below 2. After a scheduled etching time (see Table 1), samples were taken out from the beaker and transferred into distilled water for 30 min to remove the etchants. The samples were further immersed in 2 wt% sodium hydroxide (NaOH) for 30 min to remove the tungsten oxides (WO_3), which is possibly formed due to the hydrogen evolutional corrosion. At the end, the samples were cleaned in distilled water for several times and dried by the warm air. Visual inspection shows that the as-etched samples lose their metallic luster and exhibit noticeable cracks, blisters and delaminations.

For observing the microstructure, a scanning electron microscope (SEM, *LEO 1525, Carl Zeiss GmbH, Germany*) equipped with an energy dispersive X-ray spectrometer (EDX) was utilized. Here, the surface of porous metals for SEM observation was obtained by mirror polishing before etching. To unveil the microstructure beneath the surface, a femtosecond laser system [33] was used to produce cross-sections of the specimen. The laser system contains an integrated femtosecond laser (*OneFive Origami 10XP*) to allow a fast processing of arbitrary structures and a focused ion beam (FIB) column (*Orsay Physics Ga^+ ion FIB*) to offer a precise rework. The overall composition of the investigated materials was determined by EDX analysis.

The mechanical response of the created foams under compressive stress was investigated by depth-sensing nanoindentation and Vicker's microhardness (*Buehler MacroMet® 5100 Series, Japan*) measurements. For the nanoindentation, a G200 Nanoindenter (*KLA Corporation, USA*) equipped with a Berkovich tip (*Synton-MDP, Switzerland*) is utilized. All indentations were carried out at RT on the surfaces of the specimens that had been polished before etching. Nine nanoindentation tests performed with a constant strain rate of 0.05 s^{-1} were conducted on each specimen. The continuous stiffness measurement (CSM) method was applied to track hardness as a function of the indentation depth. Vickers' microhardness performed with 10 s holding was used as an indication for the deformability and bonding strength of the W ligaments.

Experimental results

Microstructure evolution

Fig. 1a-c shows the surface microstructure of the starting material after etching in the $FeCl_3$ solution for various etching time. The etched surface exhibits an etching-time-dependent microstructure. After 2 h etching it is characterized by cellular ligaments (Fig. 1a). As the etching time prolongs to 4 h, the surface is covered by flaky ligaments with a length of 160 nm on average. The length of these flaky ligaments increases to 280 nm when further prolonging the etching time to 18 h. Together with the ligament growth, the number of cracks, blisters and delaminations or even fragmentation increases (see insert image in Fig. 1c). As shown in Fig. 1d, only W is identified by EDX for each as-

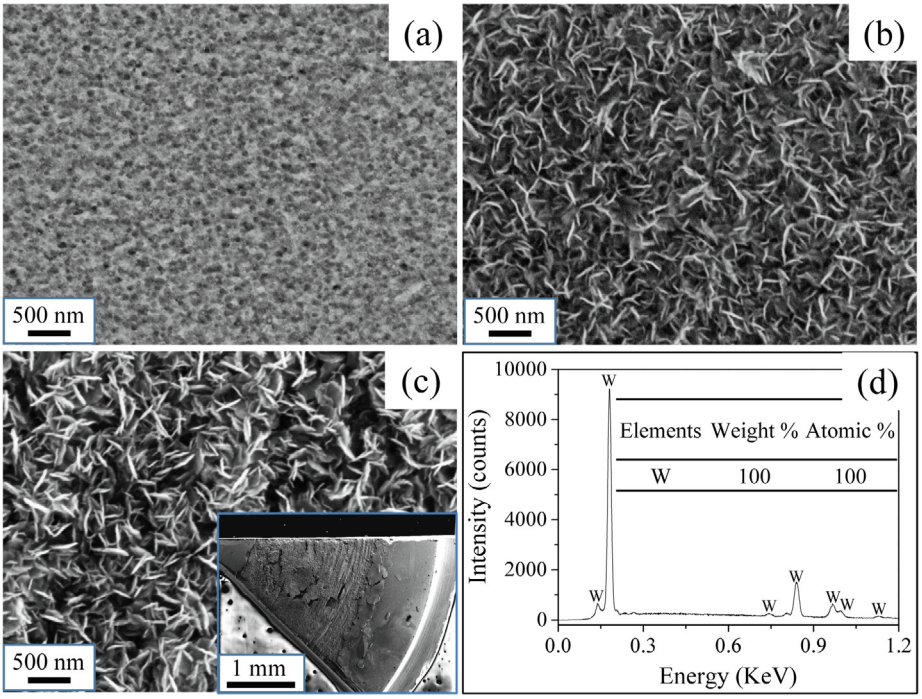

Fig. 1. Surface microstructure of as-etched nc W-Cu in $FeCl_3$ (pH < 2) solutions for various time durations: (a) 2 h. (b) 4 h. (c) 18 h. The insert image in (c) shows the surface structure of an 18 h etched 1/6 HPT sample. The bright areas in the insert image are Cu tapes. (d) shows an representative EDX analysis of the surface structures in the entire regions of (a-c). Only W is detected in the EDX spectrum.

etched surface, indicating a complete removal of Cu in the surface region.

To unveil the possible influence of HCl solution on the resulting peculiar porous structure, the specimens etched for 1 and 2 h in the $FeCl_3$ solution were further immersed in diluted HCl solution (pH = 2) for 18 h. Note that the 1 h etched sample exhibits a surface of cellular ligaments similar to the 2 h etched one (see Fig. 1a). After 18 h immersing in the diluted HCl solution, the cellular ligaments on 2 h etched specimen evolved into flaky ones and the average ligament length increased to ~ 480 nm (Fig. 2a), which is much bigger than the ligaments on the surface of 18 h $FeCl_3$ etched specimen. On the 1 h etched specimen, aggregates of flaky ligaments are observed after the further immersing in the diluted HCl solution (Fig. 2b and 2c). It reveals that the ligament structure evolves with nucleation and aggregation of new W grains. The aggregation process of new grains causes the depletion of W in certain areas. From the surface morphology of the 2 h etched specimen, it is deduced that the depletion areas can be further filled by other aggregates of W ligaments, once there are more W atoms participating in the movement along the metal/solution interfaces.

As the goal is to create a np bulk material, the depth-depended evolution of porosity is analyzed in Fig. 3. Fig. 3a and b show a femtosecond laser processed and a FIB repolished cross-sections, respectively. The position of the observed cross-sections on the 1/6 HPT specimen is schematically displayed in Fig. 3c. Two layers with different laser machining morphologies are well distinguishable in Fig. 3a, which are probably caused by different ablation characteristics of nc W-Cu and porous W. The etching front located in a depth of ~15 μm is parallel to the specimen surface, demonstrating a uniform dissolution of Cu and permeation of the etching solution over the observed area. EDX analysis shows that Cu is absent in the upper layer (i.e., as-etched region), revealing that the created W foam is entirely open cell. After reworking the cross-section with FIB, the pores (dark contrast) which are uniformly distributed in the W matrix (bright contrast) are clearly observed. A quantitative measurement shows that these pores have a size of ~ 10–30 nm, which is comparable to the size of Cu particles (20 nm) in the nanocrystalline W-Cu precursor, but much smaller than the pores observed on the sample surface (see Fig. 1c). Such small pores are probably correlated with the depth-depended Cu etching and W grain reconstruction procedures. To unveil the nanoporous structure along the cross-section, microstructure observations in the transmission electron microscopy (TEM) are required. However, the fabrication of TEM specimens turned out to be very challenging under the present conditions of a very thin foam layer (~15 μm) and depth-depended porous structures. Therefore, a detailed characterization of the nanoporous structure is not presented here.

Porosity is strongly correlated to the foam mechanical behavior as discussed in the following. However, due to the W grain reconstruction and the peculiar foam morphology, it is problematical to make a direct calculation of the porosity from the amount of Cu in the W matrix (35 vol%), or to measure the porosity simply from a two-dimensional SEM image. Given the formation and gradual evolution of cracks, blisters and delaminations at the sample surface (see Fig. 1), it is deduced that the porosity is higher than 35 vol%. At larger sample depth, where Fig. 3b represents for, the foam seems to have a porosity

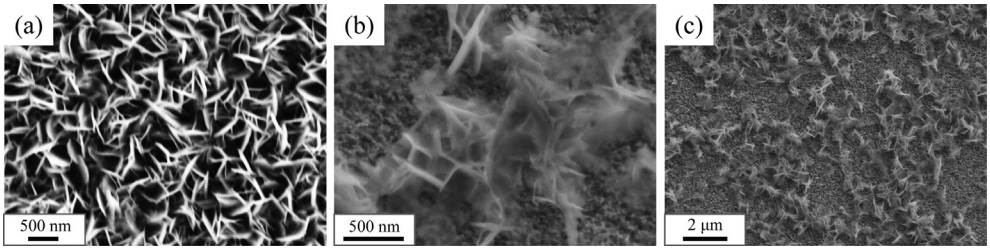

Fig. 2. Surface microstructure of as-etched nc W-Cu in $FeCl_3$ (pH < 2) solution for (a) 2 h, or (b, c) 1 h and subsequent immersing in HCl for 18 h in both cases. (b) is a high magnification SEM image, showing the details of the W flaky aggregates in (c).

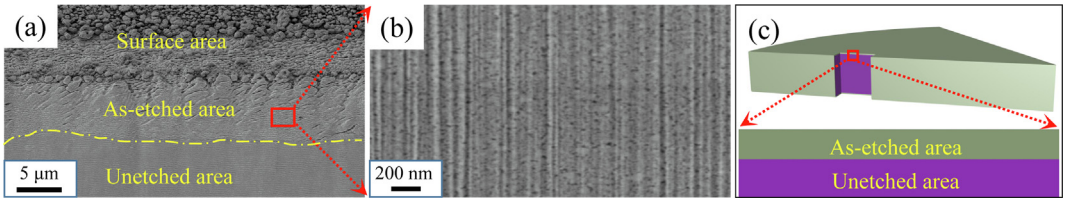

Fig. 3. Cross-sections of 18 h etched nc W-Cu precursors in $FeCl_3$ (pH < 2): (a) Femtosecond laser cut cross-section. The etching front is marked by a dashed yellow line. (b) FIB reworked detailed cross-section. (c) Schematic drawing showing the location of the observed surface region.

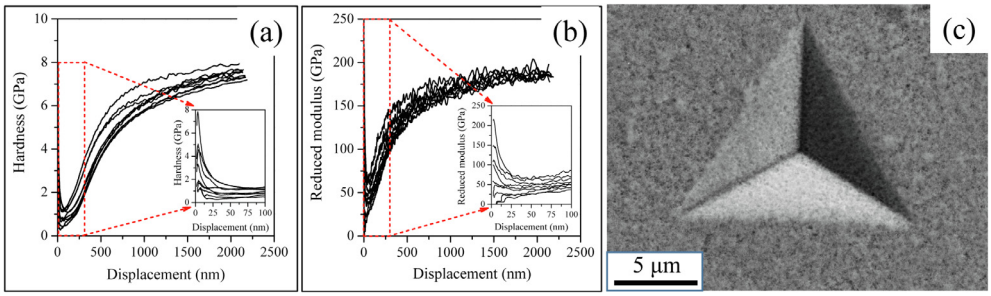

Fig. 4. Nanoindentation at a load of 670 mN on the surface of 4 h etched specimen: (a) Hardness versus displacement curves. (b) Reduced modulus versus displacement curves. (c) A representative residual indentation impression.

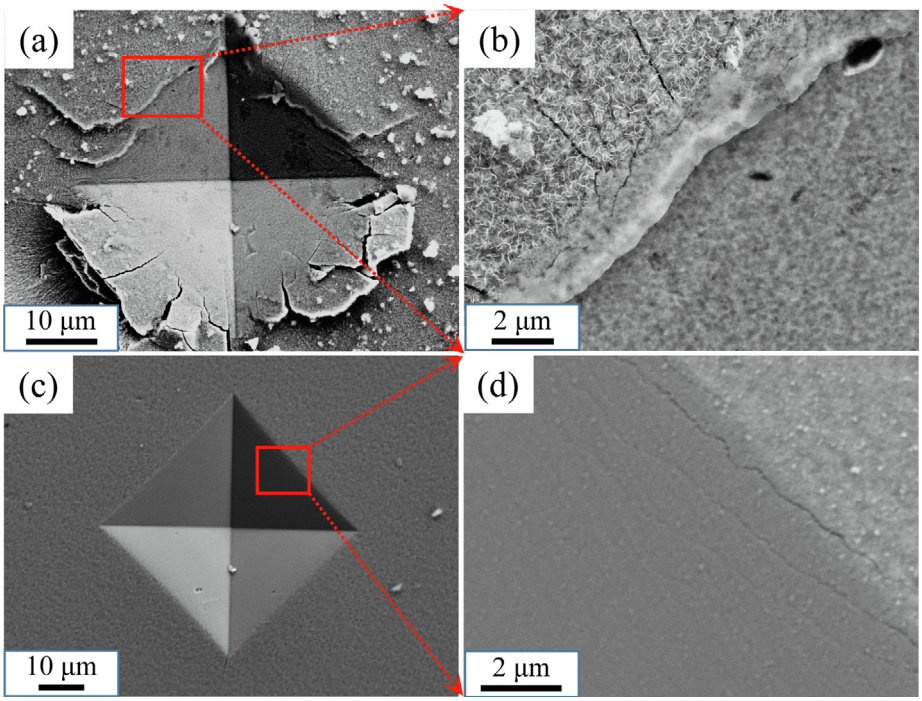

Fig. 5. Residual indentation impressions of Vicker's microhardness measurements at a load of 10 N on the surface of: (a-b) 4 h $FeCl_3$ etched specimen. (c-d) 18 h $(NH_4)_2S_2O_8$ etched specimen. (b) and (d) are high magnification images showing details of the marked areas in (a) and (c), respectively.

comparable to the Cu volume percentage (i.e., 35 vol%).

Mechanical behavior

The nanoindentation response of a 4 h $FeCl_3$ etched specimen is displayed in Fig. 4. Hardness (H) and reduced Young's modulus (E_r), calculated by analyzing the load–displacement indentations using the Oliver-Pharr method [34], are given in Fig. 4a and b versus displacement. At the applied load of 670 mN, a maximum depth of around of 2 μm is reached, allowing us to study the mechanical response of an ensemble of ligaments and pores instead of individual ligaments [35]. The mechanical behavior of the created foam can be revealed from the indentation depths smaller than 1 μm, as the influence from the unetched substrate layer is no longer negligible at larger indentation depths. At indentation depths ranging from 30 to 100 nm, the hardness is as low as ~ 1 GPa, corresponding to a foam yield strength (σ) of 380 MPa via the constraint factor C^* by $H = C^* \cdot \sigma$. Note that the value of C^* (0.26, Ref. [29]) for the reference nanofoam was taken for the calculation of σ. In comparison to the reference nanofoam, which has a yield strength value about 2 GPa, the nanofoam tailored by using $FeCl_3$ solution has a much lower strength. The poor mechanical strength of the foam created by $FeCl_3$ etching should be dominantly controlled by the reconstructed ligament structures. The porosity, which is generally higher than the reference foam (35 vol%, Ref. [29]) may to some extent

also contribute to its poor strength. At the indentation depths below 30 nm, due to the indentation size effect or contact imperfections, the foam tends to be harder than 1 GPa. With the increase of the indentation depths from 100 nm, the hardness of the created porous W increases initially fast and then saturates at indentation depths above 1 μm. The reduced Young's modulus shown in Fig. 4b exhibits a changing trend similar to the hardness, i.e., E_r increases rapidly from ~ 60 GPa at indentation depths ~ 100 nm and saturates at a value of 180 GPa. Note that 180 GPa is much smaller than the E_r of solid nanocrystalline W (335.8 GPa, Ref. [29]), revealing its porous nature during the indentation process. Residual indentation impression in Fig. 4c shows that deformation of the created foam is contained in the contact area without material pileup or deformation adjacent to the residual impression. Research of Leitner et al. [36] suggests that the created foam deformed via a collapsing and compacting of the evolved peculiar ligaments (i.e. densification), thus leading to the increase of hardness and Young's modulus for indentation depths between 100 nm and 1 μm.

Fig. 5 shows residual impressions of Vicker's Microhardness tests on the 4 h $FeCl_3$ etched specimen surface. Indentation impressions on the surface of 18 h $(NH_4)_2S_2O_8$ etched specimen are taken as a reference. For the fabrication and microstructure details of the 18 h $(NH_4)_2S_2O_8$ etched specimen, please refer to Ref. [29]. At the load of 10 N, indentation depths around 8.8 and 10.6 μm were calculated for the $FeCl_3$ and the $(NH_4)_2S_2O_8$ etched specimens, which correspond to approximately 60 and 70% of the total thickness of the as-etched layers, respectively. Such deep indentation depths give rise to the issue of substrate effects. Thus, the Vicker's hardness values are no longer reliable and will not be discussed. As seen from Fig. 5, severe cracking and fracturing are observed around the indentation impression of the $FeCl_3$ etched specimen, while only minor cracks are noticed in the indentation impression of np W tailored by using $(NH_4)_2S_2O_8$. This behavior is in good agreement with the nanoindentation tests, which unveils that the ligament strength in the nanofoam created by using $FeCl_3$ solution is much weaker than the nanofoam created in $(NH_4)_2S_2O_8$ solution.

Discussion

As described above, when using $FeCl_3$ as etchant, equiaxed W grains in the nc W-Cu starting material evolved into peculiar W ligaments due to grain reconstruction, including grain nucleation, aggregation and growth. This grain reconstruction behavior can be described by the solid/liquid interface diffusion mechanism, which has been widely proposed to explain the nucleation and growth processes of ligaments of np metals during dealloying of crystalline precursors [19,37-40]. As described by the Arrhenius equation given below, the diffusion of metal atoms along the metal/solution interfaces is a thermally activated process [41]:

$$D_s = D_0 \exp\left[- \frac{\Delta H_S^*}{RT} \right] \quad (1)$$

where D_s is the surface diffusion coefficient, D_0 is the pre-exponential factor taken as a constant, R is the gas constant, T is the etching temperature, and ΔH_S^* is the activation enthalpy for the surface diffusion process. The activation enthalpy ΔH_S^* is composed of two parts, ΔH_F^* and ΔH_D^*, representing the activation enthalpies for forming the moving entities and their diffusion process, respectively [41]. A list of intrinsic diffusion parameters for W on three different W crystal planes at RT is given in Table 2. Note that Table 2 does not contain all data available in the literature. The variation in D_s values for W along different crystal planes gives an explanation for the formation of anisometric ligaments, i.e., flaky ligaments. In experiments where the D_s was determined, the calculation of ΔH_S^* and D_0 was derived from the slope and intercept (extrapolation to infinite temperature) of an Arrhenius plot. Therefore, the ΔH_S^* and D_0 listed in Table 2 are with certain errors. To simplify the calculation as well as to minimize the errors, the average D_s and ΔH_S^* for W intrinsic diffusion are determined from the listed intrinsic diffusion systems by neglecting their changes with crystal planes.

Table 2
Intrinsic diffusion parameters for W on different crystal planes at room temperature [42].

System	D_0 ($\times 10^{-4}$ cm^2/s)	ΔH_S^* (kJ/mol)	D_s ($\times 10^{-18}$ cm^2/s)	Ref.
W/W(1 1 0)	10.0	83.7	3.3	[43]
W/W(1 1 0)	26.0	87.9	1.6	[43]
W/W(1 1 0)	62.0	87.9	3.8	[44]
W/W(2 1 1)	15.0	82.5	8.1	[43]
W/W(3 2 1)	4.0	83.7	1.3	[43]
W/W(3 2 1)	12.0	81.2	11.0	[45]
Average W/W		84.5	4.8	This work

Referring to the isothermal grain growth in polycrystalline materials [46], the interplay between ligament radius r and the dealloying conditions can be modeled using the following diffusion equation [47]:

$$\frac{d(r^4)}{dt} = \frac{32\gamma a^4 D_s}{kT} \quad (2)$$

where γ is the surface free energy, a is the lattice parameter, and t is the dealloying time. Integration of Eq. (2) between r_0 and r, for $t = 0$ and $t = t$, respectively, leads to

$$r(t) = \left[r_0^4 + \frac{32\gamma a^4 D_s t}{kT} \right]^{1/4} \quad (3)$$

where r_0 represents the radius of the coalescing particle at $t = 0$. In the case of our work, r_0 is taken as the ligament length measured for 4 h etched specimen (Fig. 1b). Eq. (3) allows a quantitative determination of D_s from the experimentally measured ligament lengths. Values for parameters in Eq. (3) are listed in Table 3. Note that 2500 ergs/cm^2 is an average energy value for γ, which neglects the fact that its magnitude changes with crystal planes [48] or the etching solution. A D_s value of 5.7×10^{-16} cm^2/s is therefore calculated by using Eq. (3). In comparison to the intrinsic diffusion coefficient (4.8×10^{-18} cm^2/s), the surface diffusivity of W atoms in the used $FeCl_3$ solution is thereby accelerated by two orders of magnitude. According to Eqs. (1) and (3), the changes of ΔH_S^* and r as a function of the varying D_s are displayed in Fig. 6. It is clearly seen such a prominent increase of D_s corresponds to a ΔH_S^* reduction of about 15%, i.e., from 84.5 to 72 kJ/mol, which should be due to the interaction between solvent ions and the surface W atoms [41,49]. Moreover, it is noticed from Fig. 6 that no ligament growth is noticeable when D_s is lower than 1×10^{-17} cm^2/s, or when ΔH_S^* decreases by less than 2%. From the perspective of thermodynamics, this finding provides a good explanation for the case of using $(NH_4)_2S_2O_8$ as etchant [29], in which no grain modifications were observed. It unveils that the influence of $(NH_4)_2S_2O_8$ solution on the ligament structure is negligible because the interaction of solvent ions in $(NH_4)_2S_2O_8$ solution with the surface W atoms is extremely weak or even absent.

The question remains as to which ions exactly interact with the surface W atoms. As described in Section 3.1, cellular ligaments on the 2 h etched surface evolved into flaky ligaments in both acidified $FeCl_3$ and diluted HCl solution. It shows that H^+ or Cl^- ions, which exist in both solutions, are possibly the interacting ions. But H^+ ions are excluded, as in $(NH_4)_2S_2O_8$ solution, where H^+ with a concentration

Table 3
Values of parameters used for the calculation of surface diffusion coefficient of W atoms (D_s) in the used $FeCl_3$ etching solution.

γ (ergs/cm^2)	a (cm)	T (K)	t (h)	t_0 (h)	r (nm)	r_0 (nm)
2500	3.16×10^{-8}	300	18	4	280	160

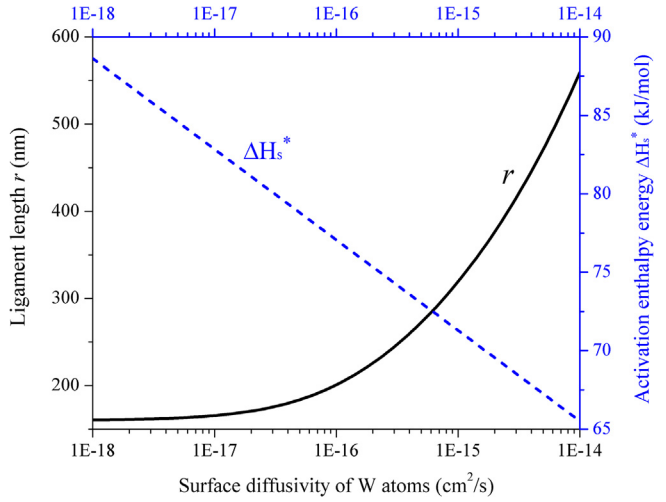

Fig. 6. Plots of r vs D_s based on Eq. (3) and ΔH_S^* vs D_s based on Eq. (1). Length of ligaments on 4 h etched sample surface, i.e., 160 nm, is taken as the initial ligament length.

comparable to the diluted HCl solution (i.e. both solutions have a pH of 2) exists due to the hydrolysis of $(NH_4)_2S_2O_8$ [29], surface moving entities diffuse with a speed probably smaller than 1×10^{-17} cm^2/s according to Fig. 6, as no ligament evolution was observed. Therefore, it is concluded that W surface diffusion is drastically facilitated by the interaction between Cl^- ions and surface W atoms. This conclusion is also in good accordance with reports showing that Cl^--containing solutions (e.g. neutral NaCl solution [21,50], or acidic HCl solution [51,52]) have an acceleration effect on the surface diffusion of the noble Au during dealloying.

A common feature accompanied with dealloying is the formation of cracks within the np metals [53-55]. The cracking phenomenon during dealloying is generally regarded as a result of the rate of stress increase resulting from the removal of active atoms overweighing the rate of stress relief from surface diffusion of remaining atoms [56]. When using $FeCl_3$ as the etchant, the stress increase rate seems to be faster than the stress relief rate. Unveiled by the indentation tests, the created ligaments are not strong enough to withstand the residual internal stress, causing ultimately the formation of cracks in the as-etched layer. Accompanying with the cracks, blisters and delaminations are observed in the as-etched layer as well. Formation of the blisters is probably correlated with the grain nucleation and aggregation processes, while appearance of the delaminations can be interpreted by the mechanical mismatch between different ligament structures.

Conclusions

We aimed at creating a tungsten nanofoam by selective phase dissolution from nanocrystalline W-Cu in an $FeCl_3$ solution, exploring its porous structure evolution behavior during the selective dissolution process and its mechanical response under compressive stress. The Cu phase turned out to be selectively removed in the used $FeCl_3$ solution, leading to a successful formation of nanoporous tungsten. However, the formed porous structure was unstable. Its ligaments evolved from a cellular to a flaky structure with the prolonging of etching time.

Observation of cellular ligament evolution in the acidified $FeCl_3$ solution and the diluted HCl solution showed that Cl^- ions can reduce the activation enthalpy for W surface diffusion by interacting with W atoms, thus accelerating the mobility of W atoms. Based on the surface-diffusion controlled coarsening mechanism, the surface diffusion coefficient of W atoms in the used $FeCl_3$ solution was calculated as 5.7×10^{-16} cm^2/s, which is around two orders of magnitude faster than the intrinsic W diffusion value. Nanoindentation tests revealed that the created foam has a ligament strength as low as 380 MPa and deforms via a fast collapsing and compacting of the ligaments. The low ligament strength ultimately led to the formation of cracks during the etching process.

In conclusion, this work provides a novel methodology for creating nanoporous W. Combining our previous work [29], which focused on tailoring W nanofoam by using $(NH_4)_2S_2O_8$ solution, with the current results on using $FeCl_3$ as etchant, it is shown that the type of etching solution significantly influences the resulting W porous structures. Due to the nanocrystalline nature of the W-Cu precursors, it is hardly to produce W foam layers above a thickness of tens of microns. The low ligament strength in the present case also limits the use of the created foam in structural applications. However, the created W foams are nanostructured and entirely open cell, thus having a potential to be used as high current density cathodes. In addition, the fast surface diffusion characteristics of W atoms in Cl^--containing solutions provide an unique way to tailor porous W materials with various structural parameters, such as ligament shapes and sizes, for engineering applications requiring different physical, mechanical and other properties. For instance, due to the exceptional resistance of W to melting, W foam foils can be used to filter high temperature liquid and gas in aerospace, power electronics and metallurgical industries. The filtering speed meanwhile can be adjusted by increasing/decreasing the layers of the thin foam foils, variable ligament shapes and sizes.

Author contributions

M.Z. designed the experiment, fabricated the materials and conducted the microstructure characterization and data analysis. M.J.P. performed the cutting and SEM imaging of the cross-section (Fig. 4). This work was carried out under the supervision of D.K. M.Z. wrote the original paper draft. D.K. and M.J.P. reviewed the draft paper and offered many valuable suggestions to modify the draft paper.

CRediT authorship contribution statement

Mingyue Zhao: Conceptualization, Methodology, Investigation, Writing - original draft, Visualization, Project administration, Funding acquisition. **Manuel J. Pfeifenberger:** Writing - review & editing. **Daniel Kiener:** Writing - review & editing, Supervision.

Declaration of Competing Interest

The authors declare that they have no known competing financial interests or personal relationships that could have appeared to influence the work reported in this paper.

Acknowledgments

This work is funded by the Austria Science Fund (FWF) under the Lise Meitner project M 2405-N36 (IRRESIST). D.K. kindly acknowledges financial support by the European Research Council (ERC) under grant No. 771146 (TOUGHIT). The authors would like to thank Michael Wurmshuber for conducting nanoindentation tests.

Appendix A. Supplementary data

Supplementary data to this article can be found online at https://doi.org/10.1016/j.rinp.2020.103062.

References

[1] P.S. Liu, G.F. Chen, Chapter Three - Application of Porous Metals, in: P.S. Liu, G.F. Chen, Porous Materials. first ed., Butterworth-Heinemann, Boston, 2014, pp. 113–188.
[2] Gibson LJ, Ashby MF. Cellular solids, structure and properties. second ed.

Cambridge (UK): Cambridge University Press; 1997.
[3] Setyawan W, Kurtz RJ. Effects of transition metals on the grain boundary cohesion in tungsten. Scr. Mater. 2012;66:558–61. https://doi.org/10.1016/j.scriptamat.2012.01.002.
[4] Selcuk C, Bentham R, Morley N, Wood JV. Microhardness as a measure of homogeneity of porous tungsten. Mater. Lett. 2004;58:1873–6. https://doi.org/10.1016/j.matlet.2003.11.031.
[5] Kobayashi S, Hosoda N, Takashima R. Tungsten alloys as radiation protection materials. Nucl. Instrum. Methods A 1997;390:426–30. https://doi.org/10.1016/S0168-9002(97)00392-6.
[6] Xue YF, Cai HN, Wang L, Wang FC, Zhang HF. Dynamic compressive deformation and failure behavior of Zr-based metallic glass reinforced porous tungsten composite. Mater. Sci. Eng. A 2007;445:275–80. https://doi.org/10.1016/j.msea.2006.09.025.
[7] Selcuk C, Wood JV. Reactive sintering of porous tungsten: a cost effective sustainable technique for the manufacturing of high current density cathodes to be used in flash lamps. J. Mater. Proc. Technol. 2005;170:471–6. https://doi.org/10.1016/j.jmatprotec.2005.05.037.
[8] Melnikova IP, Vorozheikin VG, Usanov DA. Correlation of emission capability and longevity of dispenser cathodes with characteristics of tungsten powders. Appl. Surf. Sci. 2003;215:59–64. https://doi.org/10.1016/S0169-4332(03)00289-7.
[9] Xu S, Bourham M, Rabiei A. A novel ultra–light structure for radiation shielding. Mater. Design 2010;31:2140–6. https://doi.org/10.1016/j.matdes.2009.11.011.
[10] Tajmar M, Vasiljevich I, Grienauer W. High current liquid metal ion source using porous tungsten multiemitters. Ultramicroscopy 2011;111:431–4. https://doi.org/10.1016/j.ultramic.2010.11.026.
[11] Lv Y, Yu X, Tan C, Ma H, Zheng J, Wang F, et al. Deposition temperature effects on tungsten single-crystal layer by chemical vapor transport. J. Cryst. Growth. 2011;329:62–6. https://doi.org/10.1016/j.jcrysgro.2011.06.040.
[12] Li Y, Yu X, Tan C, Wang F, Ma H, Yue J. Porous tungsten prepared by atmospheric-pressure chemical vapor deposition with WF_6 and its characterization. AIP Conf Proc 2017;1839:20007. https://doi.org/10.1063/1.4982372.
[13] Shen Q, Zhou D, Zhang J, Luo G, Zhang L. Study on preparation and property of porous tungsten via tape-casting. Int. J. Refract. Met. Hard Mater. 2017;69:27–30. https://doi.org/10.1016/j.ijrmhm.2017.07.018.
[14] Volkert CA, Lilleodden ET, Kramer D, Weissmüller J. Approaching the theoretical strength in nanoporous Au. Appl. Phys. Lett. 2006;89:61920. https://doi.org/10.1063/1.2240109.
[15] Hodge AM, Biener J, Hayes JR, Bythrow PM, Volkert CA, Hamza AV. Scaling equation for yield strength of nanoporous open-cell foams. Acta Mater. 2007;55:1343–9. https://doi.org/10.1016/j.actamat.2006.09.038.
[16] Bringa EM, Monk JD, Caro A, Misra A, Zepeda-Ruiz L, Duchaineau M, et al. Are Nanoporous Materials Radiation Resistant? Nano Lett. 2012;12:3351–5. https://doi.org/10.1021/nl201383u.
[17] Li J, Fan C, Ding J, Xue S, Chen Y, Li Q, et al. In situ heavy ion irradiation studies of nanopore shrinkage and enhanced radiation tolerance of nanoporous Au. Sci. Rep. 2017;7:39484. https://doi.org/10.1038/srep39484.
[18] Sun C, Bufford D, Chen Y, Kirk MA, Wang YQ, Li M, et al. In situ study of defect migration kinetics in nanoporous Ag with enhanced radiation tolerance. Sci. Rep. 2014;4:3737. https://doi.org/10.1038/srep03737.
[19] Erlebacher J, Aziz MJ, Karma A, Dimitrov N, Sieradzki K. Evolution of nanoporosity in dealloying. Nature 2001;410:450. https://doi.org/10.1038/35068529.
[20] Ding Y, Kim YJ, Erlebacher J. Nanoporous gold leaf:"Ancient technology"/advanced material. Adv. Mater. 2004;16:1897–900. https://doi.org/10.1002/adma.200400792.
[21] Zhang Q, Wang X, Qi Z, Wang Y, Zhang Z. A benign route to fabricate nanoporous gold through electrochemical dealloying of Al-Au alloys in a neutral solution. Electrochim. Acta 2009;54:6190–8. https://doi.org/10.1016/j.electacta.2009.05.089.
[22] Zhang C, Sun J, Xu J, Wang X, Ji H, Zhao C, et al. Formation and microstructure of nanoporous silver by dealloying rapidly solidified Zn–Ag alloys. Electrochim. Acta 2012;63:302–11. https://doi.org/10.1021/jp902490u.
[23] Luo X, Li R, Huang L, Zhang T. Nucleation and growth of nanoporous copper ligaments during electrochemical dealloying of Mg-based metallic glasses. Corros. Sci. 2013;67:100–8. https://doi.org/10.1016/j.corsci.2012.10.010.
[24] Wada T, Setyawan AD, Yubuta K, Kato H. Nano- to submicro-porous β-Ti alloy prepared from dealloying in a metallic melt. Scr. Mater. 2011;65:532–5. https://doi.org/10.1016/j.scriptamat.2011.06.019.
[25] Wada T, Yubuta K, Inoue A, Kato H. Dealloying by metallic melt. Mater. Lett. 2011;65:1076–8. https://doi.org/10.1016/j.matlet.2011.01.054.
[26] McCue I, Ryan S, Hemker K, Xu X, Li N, Chen M, et al. Size effects in the mechanical properties of bulk bicontinuous Ta/Cu nanocomposites made by liquid metal dealloying. Adv. Eng. Mater. 2015;18:46–50. https://doi.org/10.1002/adem.201500219.
[27] Wada T, Ichitsubo T, Yubuta K, Segawa H, Yoshida H, Kato H. Bulk-nanoporous-silicon negative electrode with extremely high cyclability for lithium-ion batteries prepared using a top-down process. Nano Lett. 2014;14:4505–10. https://doi.org/10.1021/nl501500g.
[28] Kosmidou M, Detisch MJ, Maxwell TL, Balk TJ. Vacuum thermal dealloying of magnesium-based alloys for fabrication of nanoporous refractory metals. MRS Commun. 2019;9:144–9. https://doi.org/10.1557/mrc.2019.15.
[29] Zhao M, Issa I, Pfeifenberger MJ, Wurmshuber M, Kiener D. Tailoring ultra-strong nanocrystalline tungsten nanofoams by reverse phase dissolution. Acta Mater. 2020;182:215–25. https://doi.org/10.1016/j.actamat.2019.10.030.
[30] Kormout KS, Pippan R, Bachmaier A. Deformation–induced supersaturation in immiscible material systems during high–pressure torsion. Adv. Eng. Mater. 2017;19:1600675. https://doi.org/10.1002/adem.201600675.
[31] Sabirov I, Pippan R. Formation of a W–25% Cu nanocomposite during high pressure torsion. Scripta Mater. 2005;52:1293–8. https://doi.org/10.1016/j.scriptamat.2005.02.017.
[32] Oura K, Katayama M, Zotov AV, Lifshits VG, Saranin AA. Surface Science. Springer, Berlin, Heidelberg: Advanced Texts in Physics; 2003.
[33] Pfeifenberger MJ, Mangang M, Wurster S, Reiser J, Hohenwarter A, Pfleging W, et al. The use of femtosecond laser ablation as a novel tool for rapid micro-mechanical sample preparation. Mater. Design 2017;121:109–18. https://doi.org/10.1016/j.matdes.2017.02.012.
[34] Oliver WC, Pharr GM. An improved technique for determining hardness and elastic modulus using load and displacement sensing indentation experiments. J. Mater. Res. 1992;7:1564–83. https://doi.org/10.1557/JMR.1992.1564.
[35] Andrews EW, Gioux G, Onck P, Gibson LJ. Size effects in ductile cellular solids. Part II: experimental results. Int. J. Mech. Sci. 43 2001:701–13. https://doi.org/10.1016/S0020-7403(00)00043-6.
[36] Leitner A, Maier-Kiener V, Jeong J, Abad MD, Hosemann P, Oh SH, et al. Interface dominated mechanical properties of ultra-fine grained and nanoporous Au at elevated temperatures. Acta Mater. 2016;121:104–16. https://doi.org/10.1016/j.actamat.2016.08.071.
[37] Erlebacher J. An atomistic description of dealloying: porosity evolution, the critical potential, and rate-limiting behavior. J. Electrochem. Soc. 2004;151:C614–26. https://doi.org/10.1149/1.1784820.
[38] Snyder J, Asanithi P, Dalton AB, Erlebacher J. Stabilized nanoporous metals by dealloying ternary alloy precursors. Adv. Mater. 2008;20:4883–6. https://doi.org/10.1002/adma.200702760.
[39] L.H. Qian, M.W. Chen, Ultrafine nanoporous gold by low-temperature dealloying and kinetics of nanopore formation, Appl. Phys. Lett. 91 (2007) 083105-1–083105-3. https://doi.org/10.1063/1.2773757.
[40] Rugolo J, Erlebacher J, Sieradzki K. Length scales in alloy dissolution and measurement of absolute interfacial free energy. Nat. Mater. 2006;5:946. https://doi.org/10.1038/nmat1780.
[41] Dona JM, Gonzalez-Velasco J. Mechanism of surface diffusion of gold adatoms in contact with an electrolytic solution. J. Phys. Chem. 1993;97:4714–9. https://doi.org/10.1021/j100120a026.
[42] Seebauer EG, Allen CE. Estimating surface diffusion coefficients. Prog. Surf. Sci. 1995;49:265–330. https://doi.org/10.1016/0079-6816(95)00039-2.
[43] Graham WR, Ehrlich G. Surface self-diffusion of single atoms. Thin Solid Films 1975;25:85–96. https://doi.org/10.1038/222977b0.
[44] Kellogg GL, Tsong TT, Cowan P. Direct observation of surface diffusion and atomic interactions on metal surfaces. Surf. Sci. 1978;70:485–519. https://doi.org/10.1016/0039-6028(78)90428-4.
[45] Bassett DW, Parsley MJ. Field ion microscope studies of transition metal adatom diffusion on (110), (211) and (321) tungsten surfaces. J. Phys. D: Appl. Phys. 1970;3:707–16. https://doi.org/10.1088/0022-3727/3/5/309.
[46] Burke JE. Some factors affecting the rate of grain growth in metals. Trans. AIME 1949;180:73–91.
[47] Andreasen G, Nazzarro M, Ramirez J, Salvarezza RC, Arvia AJ. Kinetics of particle coarsening at gold electrode/electrolyte solution interfaces followed by in situ scanning tunneling microscopy. J. Electrochem. Soc. 1996;143:466–71. https://doi.org/10.1149/1.1836466.
[48] Zhang J, Ma F, Xu K. Calculation of the surface energy of bcc metals by using the modified embedded-atom method. Surf. Interface Anal. 2003;35:662–6. https://doi.org/10.1002/sia.1587.
[49] Ji H, Wang X, Zhao C, Zhang C, Xu J, Zhang Z. Formation, control and functionalization of nanoporous silver through changing dealloying media and elemental doping. Cryst. Eng. Comm. 2011;13:2617–28. https://doi.org/10.1039/c0ce00900h.
[50] Zhang Z, Zhang C, Sun J, Kou T. Influence of anion species on electrochemical dealloying of single-phase Al_2Au alloy in sodium halide solutions. Rsc. Adv. 2012;2:4481. https://doi.org/10.1039/c2ra20087b.
[51] Hakamada M, Mabuchi M. Nanoporous gold prism microassembly through a self-organizing route. Nano Lett. 2006;6:882–5. https://doi.org/10.1021/nl0602443.
[52] F. Renner, G. Andreas Eckstein, L. Lymperakis, A. Dakkouri-Baldauf, M. Rohwerder, J. Neugebauer, M. Stratmann, In situ scanning tunneling microscopy study of selective dissolution of Au3Cu and Cu3Au (001), Electrochim. Acta 56 (2011) 1694–1700. https://doi.org/10.1016/j.electacta.2010.09.061.
[53] Seker E, Reed ML, Begley MR. A thermal treatment approach to reduce microscale void formation in blanket nanoporous gold films. Scripta Mater. 2009;60:435–8. https://doi.org/10.1016/j.scriptamat.2008.11.027.
[54] Okman O, Kysar JW. Fabrication of crack-free blanket nanoporous gold thin films by galvanostatic dealloying. J. Alloys Compd. 2011;509:6374–81. https://doi.org/10.1016/j.jallcom.2011.02.115.
[55] Sun Y, Balk TJ. A multi-step dealloying method to produce nanoporous gold with no volume change and minimal cracking. Scripta Mater. 2008;58:727–30. https://doi.org/10.1016/j.scriptamat.2007.12.008.
[56] Sun Y, Kucera KP, Burger SA, Balk TJ. Microstructure, stability and thermo-mechanical behavior of crack-free thin films of nanoporous gold. Scripta Mater. 2008;58:1018–21. https://doi.org/10.1016/j.scriptamat.2008.01.036.